Analysis of Recent Extreme Events Measured by the Barotropic Component of the Atmosphere

H. L. TANAKA[1] and Mio MATSUEDA[2]

1: Institute of Geoscience, University of Tsukuba, and Frontier Research System for Global Change
2: Graduate School of Life and Environmental Sciences, University of Tsukuba

1. Introduction

Analysis of abnormal weather is a great concern in the medium to long-range weather forecasing. Knowing the direnct and indirect causes of the abnormal weather would lead to the improvement of the long-range forecasting. However, in most cases, the reasons of the abnormal weather or any extreme event are hiden by the complexity of the chaotic nature of the nonlinear fluid dynamics. The abnormal weather is often explained, for example, by the occurance of blocking high or an amplified planetary waves which meanders the upper-air jet stream with abnormal ridges and troughs. The true dynamical reason why the jet stream has meandered is beyond the scope of the analysis. If there is a pronounced phenomenon such as El Nino or La Nina, the direct cause of the abnormal weather is attempted to link with them using the analysis of quasi-stationary Rossby wavetrain. If there is a major volcanic eruption, the abnormal weather is attempted to explain with them by the analysis of radiative impact to the atmosphere. However, if there is no such obvious impact of external forcing to the atmosphere, the abnormal weather would be elucidated by the natural variability contained in the nonlinear fluid mechanics, and the true direct and indirect causes are in the enigma.

We wonder if the long-range forecasting for the future would be possible even without knowing the true causes for the past abnormal events. It may be an important research subject to understand to what extent the abnormal weather is explained by the natural variability of the atmosphere and the external abnormal forcing.

According to the analysis by Tanaka (2003b), most of the extreme events are induced by the low-frequency variabilities of the atmosphere such as blocking high, Arctic Oscillation (AO) and PNA-like teleconnections, which are characterized by its barotropic structure. Therefore, the dynamical understanding of those low-frequency variability may be the central subject for the long-range weather forecasting. The dynamical role of the barotropic component of the atmosphere is extensively investigated by Tanaka (1998; 2003a). According to the result of the 3-D spectral energetics analysis, any heat related baroclinic energy (available potential energy) is converted to barotropic energy when the baroclinicity is removed by the activity of the synoptic disturbances (i.e., baroclinic instability). The accumulated barotropic energy at the synoptic eddies is then transformed to planetary waves by the up-scale energy cascade under the constraint of the 2-D fluid dynamics. It is in this process when the low-frequency variabilities of amplified planetary waves cause extreme events over the hemispheric scale. Interestingly, some of the extreme events can be induced by the internal natural variability of the barotropic component of the atmosphere without a specific external forcing. Hence, we can investigate the cause of the abnormal weather within the framework of the natural variability of the 2-D fluid dynamics or the abnormal external forcing to the barotropic component of the atmosphere.

The purpose of the present study is to analyze the recent abnormal weather using a quantitative abnormality index for the barotropic component of the atmosphere over the Northern Hemisphere. We attempt to separate the cause of the extreme events in a natural variability of the 2-D fluid dynamics and/or a forced response to the barotropic component of the atmosphere. A possible link to the SST anomaly is also investigated.

In section 2 the governing barotropic model equations and the data used in this study are described. In section 3 some examples of the anomaly distributions for the barotropic component of the atmosphere, external forcing, and the SST of the same month are presented. The abnormality index is introduced in section 4 to quantify the magnitude of the respective anomalies, and the long-term time series are compared with each other to investigate the possible cause of each extreme events. Finally, in section 5 the dynamical cause of the abnormal weather is discussed in the framewor of the natural variability or the external forcing to the barotropic componet of the atmosphere.

2. Analysis method and data

2.1 Analysis method

The analysis method is based on the barotropic P-model described in Tanaka and Nohara (2001) where the external forcing of the barotropic model is evaluated as the residual of the governing eaution. A brief description of the barotropic P-model is presented here.

A system of primitive equations with a spherical coordinate of longitude λ, latitude θ, pressure p, and time t may be reduced to three prognostic equations of horizontal motions and thermodynamics for three dependent variables of $U=(u,\ v,\ \phi')^T$. Here, u and v are the zonal and meridional components of the horizontal velocity, respectively, and ϕ' is a departure of the local isobaric geopotential from the reference state geopotential ϕ_0. The superscript T denotes a transpose. Using a matrix notation, these primitive

equations may be written as

$$\mathbf{M}\frac{\partial U}{\partial t} + \mathbf{L}U = N + F, \quad (1)$$

where the left-hand side of (1) represents linear terms with matrix operators $\mathbf{M}$ and $\mathbf{L}$ and the dependent variable vector U. Refer to Tanaka (1998) for the definition of matrices $\mathbf{M}$ and $\mathbf{L}$. The right-hand side represents a nonlinear term vector N and a diabatic term vector F, which includes the zonal and meridional components of frictional forces and a diabatic heating rate.

In order to obtain a system of 3-D spectral primitive equations, we expand the vectors U and F in 3-D normal mode functions in a resting atmosphere, $\Pi_{nlm}(\lambda, \theta, p)$:

$$U(\lambda, \theta, p, t) = \sum_{nlm} w_{nlm}(t) X_m \Pi_{nlm}(\lambda, \theta, p), \quad (2)$$

$$F(\lambda, \theta, p, t) = \sum_{nlm} f_{nlm}(t) Y_m \Pi_{nlm}(\lambda, \theta, p), \quad (3)$$

where the dimensionless expansion coefficients $w_{nlm}(t)$ and $f_{nlm}(t)$ are the functions of time alone. These may be computed by the inverse Fourier transforms of U and F from the observed data.

$$w_{nlm}(t) = < U(\lambda, \theta, p, t),\ X_m^{-1}\Pi_{nlm}(\lambda, \theta, p) >, \quad (4)$$

$$f_{nlm}(t) = < F(\lambda, \theta, p, t),\ Y_m^{-1}\Pi_{nlm}(\lambda, \theta, p) > . \quad (5)$$

The subscripts represent zonal wavenumbers n, meridional indices l, and vertical indices m. The scaling matrices should be defined for each vertical index as:

$$X_m = diag(c_m, c_m, c_m^2), \quad (6)$$

$$Y_m = diag(2\Omega c_m, 2\Omega c_m, 2\Omega), \quad (7)$$

where $c_m = \sqrt{gh_m}$ is a phase speed of gravity waves in shallow water associated with the equivalent height h_m, Ω is the angular speed of the earth's rotation, and *diag* represents diagonal matrix. The expansion basis of the 3-D normal mode functions $\Pi_{nlm}(\lambda, \theta, p)$ is obtained as an eigensolution of a homogeneous partial differential equation, putting zero on the right-hand side of (1). The 3-D normal mode functions are given by a tensor product of vertical structure functions and Hough harmonics associated with the linear operators $\mathbf{M}$ and $\mathbf{L}$, respectively. They form a complete set and satisfy an orthonormality condition under a proper inner product $<, >$ representing the global mass integral.

By expanding those variables in 3-D normal mode functions, we obtain a system of 3-D spectral primitive equations in terms of the spectral expansion coefficients:

$$\frac{dw_i}{d\tau} + i\sigma_i w_i = -i\sum_{jk} r_{ijk} w_j w_k + f_i, \quad (8)$$

where $i = 1, 2, 3, ..., \tau$ is a dimensionless time scaled by $(2\Omega)^{-1}$, σ_i is the eigenfrequency of the Laplace's tidal equation, and r_{ijk} is the interaction coefficients for nonlinear wave-wave interactions calculated by the triple products of the 3-D normal mode functions. The triple subscripts are shortened for simplicity as $w_{nlm} = w_i$. There should be no confusion in the use of i for a subscript even though it is used for the imaginary unit in (8).

In the 3-D spectral representation, the vertical expansion basis functions may be divided into barotropic (m=0) and baroclinic ($m \neq$0) components. We may construct a simple spectral barotropic model, using only the barotropic components (m=0) of the Rossby modes, by truncating all the baroclinic modes and high-frequency gravity modes. Such a model is equivalent to a model predicting the vertical average of meteorological variables. The barotropic components capture the essential features of the low-frequency variability of planetary-scale motions. The spectral equation for such a barotropic model may be written as:

$$\frac{dw_i}{d\tau} + i\sigma_i w_i = -i\sum_{jk} r_{ijk} w_j w_k + s_i, \quad (9)$$

where $i = 1, 2, 3, ..., (m = 0)$, the indices of the subscripts run only for the barotropic modes. The zonal and meridional wave truncation of the present model is equivalent to rhomboidal 20 with an equatorial wall. The degree of freedom of the system is reduced enormously by these truncations. The spectral equation for such a barotropic model (9) has the same form as for the baroclinic model equation (8), except for the fact that the barotropic-baroclinic interaction appears on the right hand side. Henceforth, we designate s_i as the external forcing of the barotropic model.

2.2 Data

The data used in this study are four-times daily NCEP/NCAR reanalysis for 53 years from 1950 to 2002. The data contain horizontal winds $V = (u, v)$ and geopotential ϕ, defined at every 2.5° longitude by 2.5° latitude grid point over 17 mandatory vertical levels from 1000 to 10 hPa.

The expansion coefficients w_i are obtained by the Fourier transform of (4) from the dataset of $U = (u, v, \phi')$. In order to evaluate the external forcing, w_i is interpolated to the model's time step of one hour by cubic spline method. The external forcing s_i is then diagnostically calculated by (9) as the residual of the equation from w_i. Using the long-term history data of w_i and s_i, the monthly mean climate of $\tilde{w}_i$ and $\tilde{s}_i$ and its anomaly of w_i' and s_i' are constructed for the subsequent analysis. The atmospheric anomaly is assessed only for the Northern Hemisphere by the symmetric extention of the norhtern data to the Southeren Hemisphere.

Since the quality of the SST data before 1979 is questionable due to the lack of satellite observation, analysis is concentrated for the period from 1979 to 2002.

3. Distributions of anomalies

3.1 Extreme event for January 1963

January 1963 is known as one of the most extreme events occurred in the Northern Hemisphere.

We analyzed the hight anomaly of the barotropic component of the atmosphere over the Northern Hemisphere (hereafter referred to as barotropic height). The monthly mean anomaly of w_i in (9) is converted to the geopotential height by means of the Fourier transform in (2) to present the hight anomaly. Wind anomaly can be analyzed by the same Fourier transform, but the distribution is closely in a geostrophic balance because the gravity modes are elliminated in the analysis. A positibe hight anomaly of 240 m is located at the Iceland. Another positive anomaly of 150 m is seem at Siberia extending toward Gulf of Alaska. Negative anomalies of -90 m are seen at Japan, central Canada, and Azores.

The hemispheric distribution of the external forcing to the barotropic height is also analyzed (hereafter referred to as barotropic forcing). The monthly mean anomaly of s_i in (9) is converted to the external height forcing by means of the Fourier transform in (2). Negative and positive forcing anomalies over the western and eastern half of the Eurasian continent, respectively, imply a reduced topographic forcing associated with Tibettern Plateau. The magnitude is of the order of 40 (Units). There is no marked positive forcing around the Iceland, suggesting that the large positive height anomaly is not produced by the local response to the external forcing. The distribution of the SST anomaly for the same month is analyzed. The result shows no noticable anomaly in the SST. From this result, the abnormal weather in height and the abnormal external forcing are unlikely to be explained by the boundary forcing due to the SST anomaly.

3.2 Extreme event for January 1977

January 1977 was extreme in that an abnormal high pressure system stayed in the Arctic for a month.

We analyzed the barotropic hight anomaly for the month. A positibe hight anomaly of 420 m is located in the Arctic Ocean. The magnitude of the hight anomaly is the most extreme in the historical record in the Northern Hemisphere. A negative anomalies of -180 m is seen at the Aleutian and another one at England. The anomaly pattern corresponds to the negative AO index.

The distribution of the barotropic forcing shows negative anomalies of 30 (Units) at Siberia and the West Coast of the US. Localized positibe anomalies of 30 (Units) are seen at north Pacific and Atlantic. The magnitude of the forcing anomaly is weak. The distribution of the SST anomaly shows a typical El Nino pattern at the equatorial Pacific with the peak value of 2.0 K. The result suggests some connection between the SST anomaly and the extreme event over the Arctic Ocean through the characteristic forcing pattern. Yet, the speculation is inconclusive. The extreme event during the winter of 1977 is known to trigger the climate shift from the positive AO to negaitve AO regimes.

3.3 Extreme event for January to February 1989

The abnormal weather in January and February 1989 was extensively documented by previous studies. The monthly mean temperature at Barrow Alaska was negative in January by 3σ while that in Februrary was positive in Februrary by 4σ, where σ denotes the standard deviation of the monthly mean temperature variation. The normal probability of the 4σ corresponds to one in 10,000 events.

We analyzed the barotropic hight anomaly for January. A negative hight anomaly of 270 m occupies the Arctic region, and positive height anomalies of 150 m are seen at the Europe and the north Pacific. The anomaly pattern corresponds to the typical positive AO index.

The distribution of the barotropic forcing shows positive and negative forcing anomalies over the western and eastern frank of Tibettern Plateau, respectively, which implies an intensified topographic forcing just opposit to the case in January 1977. The magnitude is of the order of 40 (Units). The distribution of the SST anomaly shows a typical La Nina pattern at the equatorial Pacific with the peak value of -2.5 K.

The subsequent February shows similar positive AO index pattern except for the pronounced positive height anomaly at the West Coase of the US. During almost a month, a series of blocking highs were created around Alaska to cause an abnormal warm spell. A heat budget analysis for the abrupt shift from the cold spell to warm spell in Alaska was reported by Tanaka and Milkovitch (1990), indicating the persistent adiabatic warming due to the downward motion associated with the blocking high.

The distribution of the barotropic forcing shows similar topographic forcing pattern at the Eurasian continent. A notable difference of enhanced positive anomaly is seen at the nort of Alaska which explains the direct positive forcing of the positive height anomaly. The magnitude is of the order of 40 (Units). We analyzed the distribution of the SST anomaly in Feburary with a typical La Nina pattern. The equatorial SST anomaly is slightly reduced to -2.0 K.

It is noteworthy that the same La Nina pattern has resulted in an extreme cold January and an extreme warm February in Alaska. The result suggests a complicated atmospheric response to the SST anomaly which is not explained by a simple linear theory. The extreme event during the winter of 1989 is known to trigger the climate shift from the negative AO to positive AO regimes.

3.4 Extreme event for April 1997

Finally, an example of abnormal weather in Spring is presented here. In general, the atmospheric anomaly is larger in winter than in summer. Some normalization is necessary to compare the magnitude of anomaly in different seasons. April 1997 was a typical case of an exceptionally large anomaly for this season.

We analyzed the barotropic hight anomaly for April 1997. A negative hight anomaly of 210 m occupies the Arctic region extending to the Mediteranean and to the north Pacific. Positive height anomalies of 120 m are seen at the north Atlantic and Siberia.

The opposit signs of anomaly at the north Pacific and Atlantic is similar to the second EOF pattern in the Northern Hemisphere as documented by Tanaka (2003b).

The distribution of the barotropic forcing shows positive and negative forcing anomalies over the Europ and west Siberia with the magnitude of 40 (Units). The forcing is out of phase with that in the hight pattern, and tends to damp the anomaly. Thus, the anomaly ought to be excited by the nonlinear dynamical process internal to the atmosphere in (9). The distribution of the SST anomaly illustrates the beginning of the largest El Nino event during 1997/1998.

It is interesting to note that an abnormal height pattern took place in April 1997 just before the beginning the largest El Nino event. Although the magnitude of the anomaly is comparable with that in the winter season, the normalized abnormality for this month will appear to be the largest in the recent 50 years.

4. Abnormality indices

4.1 Atmospheric anomaly

In this section, the abnormality of the anomaly in the barotropic atmosphere presented in section 3 is quantified to investigate the relative magnitude of the anomaly and to see its long-term variations. One of the reasonable quantificationa of the intensity of the anomaly over the hemisphere may be calculating the variance of the anomaly over the northern domain.

As discussed by Tanaka (2003b), total energy E of the atmosphere (sum of kinetic energy and available potential energy) is simply the sum of the energy elements E_i defined by:

$$E_i = \frac{1}{2} p_s h_m |w_i|^2, \tag{10}$$

where w_i is the state variables in (9), p_s is the mean surface pressure, and h_m is the equivalent depth of the vertical mode m. The value must be divided by 2 for zonal components. The magnitude of the atmospheric anomaly can be measured by the same energy norm replacing w_i by its anomaly w_i'. Since only the barotropic component (m=0) is considered in this study, we disregard the scaling parameters of $p_s h_m$ for simplicity and define the atmospheric anomaly index E_A by the following dimensionless form:

$$E_A = \sum_i \frac{1}{2} |w_i'|^2, \tag{11}$$

where the summation is taken over the all state variables. The anomaly index is calculated for the monthly mean data, so the contributions from transient eddies are not included.

We analyzed the time series of the atmospheric anomaly index for 1979 to 2002. The magnitude of the anomaly in section 3 is quantified by the energy norm in (11). If the values are multiplied by $p_s h_m (\sim 10^9)$, the units become J m^{-2}. Note that not only the height variance (available potential energy) but also the wind variance (kinetic energy) of the anomaly are counted for this index. The result shows larger anomalies in winter season and relatively smaller anomalies in summer season. Among those January and February 1989 are the largest, indicating the most unusual months during the last 24 years.

Although the anomaly index so defined contains the fundamental information on the abnormality, it may be more appropriate to normalize it by the climatological mean value for every month to remove the seasonal change. The number is refered to as the abnormality index for the atmosphere in this study. Figure 1 illustrates the normalized anomaly index of the barotropic component of the atmosphere for 1979 to 2002. The abnormality index varies around the mean of unity. The probability distribution of the variation may be regarded as Chi-squared distribution with the estimated degree of freedom of 28. The abnormality index thus represents the Chi-squared value normalized by the degree of freedom. Among those, April 1997 appears to be the most unusual month during the last 24 years exceeding the months of Janaury and February 1989. The abnormality index reaches to 2.04. The probability of this Chi-squared value corresponds to one in 1000 events. The abnormality index of the atmosphere for the top 16 abnormal months during the last 50 years for 1953 to 2002 is listed in Table 1.

4.2 Forcing anomaly index

The same analysis of the quantification for the abnormal forcing anomaly is conducted in this subsection. The magnitude of the forcing anomaly can be measured by the same 2-norm as (11) replacing w_i' by s_i'. The forcing anomaly index E_F is thus defined by the following dimensionless form:

$$E_F = \sum_i \frac{1}{2} |s_i'|^2. \tag{12}$$

The value must be divided by 2 for zonal components as before.

We analyzed the time series of the forcing anomaly index for 1979 to 2002. The result shows larger anomalies in winter season and relatively smaller anomalies in summer season. Among those, the winter of 1982/83 and 1983/84 are the largest, indicating the most unusual months with respect to the forcing during the last 24 years. The winter of 1982/83 corresponds to the El Nino year, although 1983/84 is not. January and February 1989 are also large, suggesting a strong link with the abnormal winter discussed in section 3.3.

The raw value of the forcing anomaly index is normalized as before by the climatological mean value for every month to remove the seasonal change. The number is refered to as the abnormality index for the forcing. Figure 2 illustrates the abnormality index of the forcing for 1979 to 2002. The probability distribution of the variation may be regarded as Chi-squared distribution with the estimated degree of freedom of 47. The abnormality index represents the Chi-squared value normalized by the degree of freedom. Among those, February 1984 appears to be the most unusual month during the last 24 years exceeding Janaury 1983 of the El Nino winter. The abnormality index reaches to 1.63. The probability

of this Chi-squared value corresponds to one in 250 events. January and February 1989 are also large, showing the index of 1.45. Also large is the value for June 1998, which corresponds to one year after the largest El Nino event in 1997/98. The abnormality index of the forcing for the top 16 abnormal months during the last 50 years for 1953 to 2002 is listed in Table 1.

4.3 SST anomaly index

Finally, the same analysis is conducted for the quantification of the abnormal SST anomaly in this subsection. The magnitude of the overall SST anomaly is measured by the 2-norm of the SST anomaly integrated over the area of Ocean. The anomaly index so defined is normalized as before by the climatological mean value for every month to remove the seasonal change. The number is refered to as the abnormality index for the SST.

Figure 3 illustrates the time series of the normalized SST anomaly index for 1979 to 2002. The result shows two major El Nino events for 1982/83 and 1997/98. Quantitatively, the abnormality index of the El Nino event for 1997/98 is 3.6, which is clearly larger than 2.6 for 1982/83. In addition to these two extreme events, high indices are seen for summer of 1987 and for spring of 1992. The latter may corresponds to the major volcanic eruption of Mt. Pinatubo. The abnormality index shows approximately 5 year period, and is uneasy to fit with Chi-squared distribution. The La Nina event for 1988/89 is expressed by rather weak signal by this measure.

It is interesting to compare the abnormality index for the SST in Fig. 3 with the those for the atmosphere and forcing. The extreme events in the SST show persistency to the extent of about one year. Despite the persistent impact of the SST, the atmosphere and its forcing field respond rather randomly with the time scale of a month. Therefore, some atmospheric extreme events correspond to the extreme SST event, but some show no correspondence even for the same SST anomaly. The short time scale of the atmospheric extreme events may represent the dominant influence of the natural variability contained in the nonlinear 2-D fluid dynamics of the barotropic component of the atmosphere.

4.4 Scater diagram of anomaly indices

The separation of the atmospheric extreme events in a group of the pure natural variability of the atmosphere and in a group under the strong external forcing constraint may be an important research subject for the understanding the cause of the abnormal weather. An attempt for that question is conducted in this subsection by plotting the schater diagram of the abnormality indices for the atmosphere and its forcing.

The 16 top most extreme events during the 50 years from 1953 to 2002 are linted in Table 1 in the order of the abnormality score for both the atmospheric and forcing anomalies. As discussed in section 4.1, the most extreme event was April 1997 with the abnormality score of 2.04. January 1963 discussed in senction 3.1 appears to be the second, and January 1977 discussed in section 3.2 appeas to the the third. According to the list, February and January 1989 are ranked as 6th and 7th abnormal months in the historical record.

On the other hand, the most extreme forcing occurs in July 1957 with the abnormality score of 1.77 for the estimated degree of freedom of 47. The Chi-squared probability of this score is one in 1000 events. Since the data is rather old, we avoid to discuss in the detail. January 1963 appears to be the second, as discussed in section 3.1. January and February 1989 are ranked as 12th and 15th abnormal months in the historical record.

Figure 4 presents the scatter diagram of the abnormality indices for the atmosphere (absissa) versus that for the forcing (ordinate) for 50 years from 1953 to 2002. Since the anomaly index is normalized by its mean value, abnormality of 1.0 represents the usual state. On the other hand, the value of 0.0 represnts that the state coincides with climate, so it is the quite normal state which never happened. The large values of the abnormality index correspond to the abnormal or extreme events. Since the distributions are expected to obey the Chi-squared distributions with the degree of freedom of 28 for the atmospheric anomaly and 47 for the forcing anomaly, we can estimate the probability of the occurence. The dashed line at 1.56 for the atmospheric anomaly represents top 3% Chi-squared probability for the extreme events. In fact, 18 extreme events are counted beyond this threshould out of the total of 600 samples. The other dashed line at 1.42 for the forcing anomaly represents top 3% Chi-squared probability for the extreme events, and 17 extreme events are counted here. In this study, we define these dashed lines as the threshould for the abnormal and extreme events. The numbers of the extreme (and usual) events separated by the dashed lines are 15, 3, 14, and 568, respectively. According to the distribution in Fig. 4, it is noteworthy that only 3 events appear at the corner of the extreme events for both indices. These include the month of January 1963, January and February 1989 as listed in Table 1 with the symbol of asteriscs. Those months are likely to be abnormal because the external forcing was abnormal. Interestingly, 15 out of 18 extreme events are associated with usual external forcing. The result suggests that about 83% of the abnormal events are induced by the natural variability of the atmosphere with "usual" external forcing. Likewize, 14 out of 17 abnormal forcing result in usual weather. The result implies that the external forcing is the secondary importance for the occurence of the abnormal weather, which, in tern, enphasize the importance of the natural variability of the barotropic component of the atmosphere.

5. Summary and conclusions

In this study, the recent extreme events are analyzed in the dynamical framework of the barotropic component of the atmosphere. Most of the extreme events are induced by the low-frequency variabilities such as blocking high, Arctic Oscillation (AO) and PNA-like teleconnections, which are characterized by its barotropic structure. Therefore, the dynamical

understanding of those low-frequency variability under the constraint of the 2-D fluid mechanics may be the key problem for the solution. We attempted to separate the cause of the extreme events in a natural variability of the 2-D fluid dynamics and/or a forced response to the barotropic component of the atmosphere. The SST anomaly is also investigated to compare with the external forcing anomaly.

The magnitude of the anomaly of the atmosphere is measured by the energy norm of the anomaly integrated over the Northern Hemisphere. The abnormality score is then defined by normalizing the energy norm with its climate value. According to the result of the analysis, the most abnormal moth during the recent 50 years from 1953 to 2002 was April 1997 with the abnormality score of 2.04. The probability of this Chi-squared value corresponds to one in 1000 events. January 1963 appears to be the second, and January 1977 appeas to the the third. February and January 1989 are ranked as 6th and 7th abnormal months in the historical record. It is shown that January 1963, February and January 1989 are associated with abnormal external forcing to the barotropic component of the atmosphere. In this regard, those months are likely to be abnormal because the external forcing was abnormal.

However, it is found in this study that about 80% of the abnormal events are induced by the natural variability of the atmosphere with "usual" external forcing. Likewize, about 80% of abnormal external forcing result in usual weather. The result implies that the external forcing is the secondary importance for the occurence of the abnormal weather, which, in tern, enphasize the importance of the natural variability of the barotropic component of the atmosphere.

The abnormality indices of the barotropic atmosphere and its forcing are compared with that of the SST. The extreme events of the SST show persistency to the extent of about one year. Despite the persistent impact of the SST, the atmosphere and its forcing field respond rather randomly with the time scale of a month. Therefore, some atmospheric extreme events correspond to the extreme SST event, but most of the extreme events show no correspondence for the same SST anomaly. The short time scale of the atmospheric extreme events may represent the dominant influence of the natural variability contained in the nonlinear 2-D fluid dynamics of the barotropic component of the atmosphere.

The conclusion derived by this study suggests the importance of the dynamical behavior of the barotropic component of the atmosphere for the improvement of the medium to long-range forecasting.

6. Acknowledgments

The authors would like to express acknowledgments to Professors T. Yasunari, F. Kimura, and H. Ueda for their valuable suggestion and advice. Thanks are also due to Dr. A. Kitoh of MRI for his constructive comments. The authors appreciate Ms. K. Honda for her technical assistance.

References

Tanaka, H.L., 1998: Numerical simulation of a life-cycle of atmospheric blocking and the analysis of potential vortisity using a simple barotropic model. J. Meteor. Soc. Japan, 76 ,983–1008.

Tanaka, H.L., 2003a: Numerical simulation of the Arctic oscillation using a barotropic general circulation model. *Tohoku Geophys. Journal*, 36, 382–396.

Tanaka, H.L., 2003b: Analysis and modeling the Arctic Oscillation using a simple barotropic model with baroclinic eddy forcing. *J. Atmos. Sci.*, 60, 1359-1379.

Tanaka, H. L. and Kimura, K. 1996. Intensities of Hadley, monsoon, and Walker circulations in summers of 1993 and 1994. *Gross Wetter*, 35, 25–46 (in Japanese).

Tanaka, H.L. and M.F. Milkovich, 1990: A heat budget analysis of the polar troposphere in and around Alaska during the abnormal winter of 1988/89. Monthly Weather Review, 118, 1628-1639.

Tanaka, H.L. and D. Nohara, 2001: A study of deterministic predictability for the barotropic component of the atmosphere. Science Report, Inst. Geosci., Univ. of Tsukuba, 22A, 1–21.

Table 1. A list of abnormal year and months measured by atmospheric anomaly w_4' and forcing anomaly f_4' for the barotropic component of the atmosphsere during the 50 years form 1953 to 2002. The score represents the anomaly 2-norm scaled by its mean values. The asterisc denotes the month when both atmospheric anomaly and forcing anomaly are listed in the table.

	Atmospheric Anomaly				Forcing Anomaly			
1	1997	4	2.04		1956	7	1.77	
2	1963	1	1.92	*	1963	1	1.69	*
3	1977	1	1.89		1984	2	1.63	
4	1983	3	1.87		1963	5	1.62	
5	1967	4	1.86		1963	4	1.57	
6	1989	2	1.86	*	1961	8	1.56	
7	1989	1	1.82	*	1983	1	1.53	
8	1974	10	1.80		1998	6	1.49	
9	1997	10	1.76		1960	7	1.49	
10	1978	12	1.74		1959	9	1.47	
11	1987	10	1.72		1964	5	1.45	
12	2002	4	1.68		1989	1	1.45	*
13	1976	8	1.64		1984	5	1.45	
14	1992	5	1.62		1960	8	1.45	
15	1970	1	1.61		1989	2	1.44	*
16	1981	1	1.58		1986	4	1.44	
17	1997	5	1.58		1965	2	1.42	
18	1990	4	1.57		1960	3	1.40	

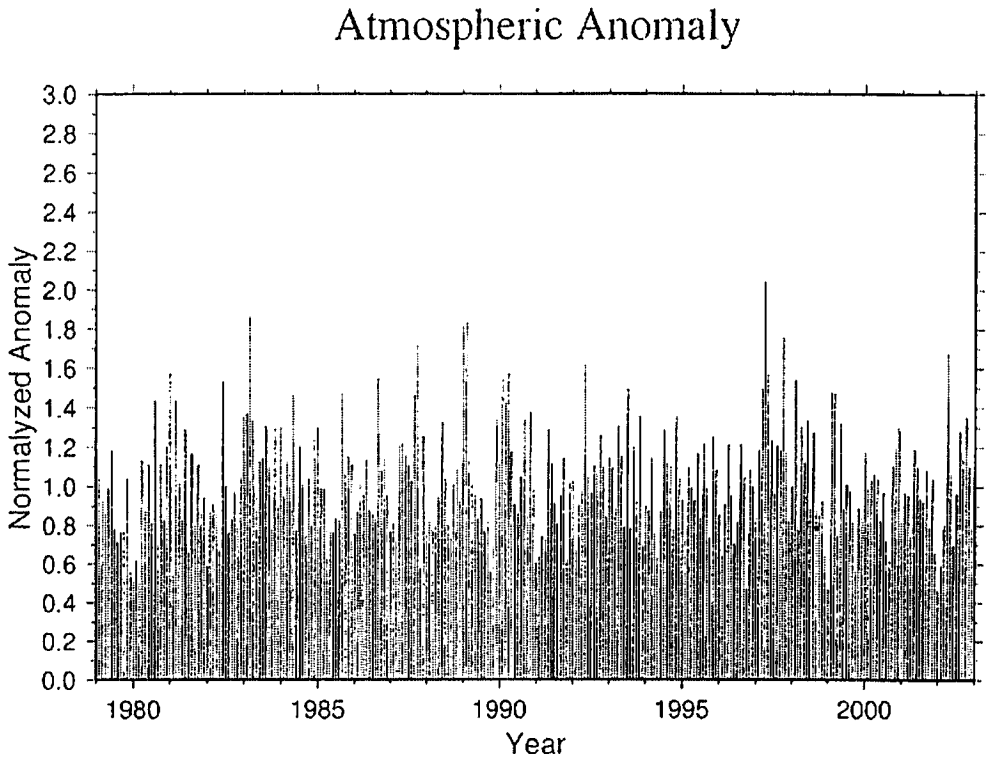

Fig. 1. The abnormality index of the barotropic component of the atmosphere for 1979 to 2002.

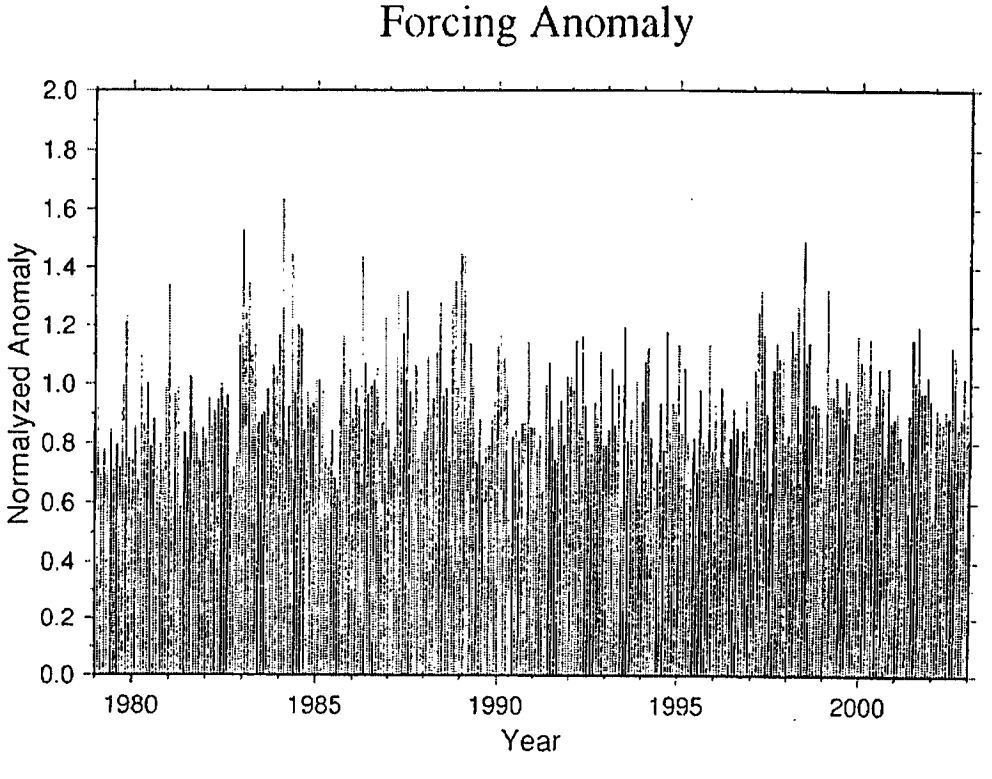

Fig. 2. The abnormality index of the forcing to the barotropic component of the atmosphere for 1979 to 2002.

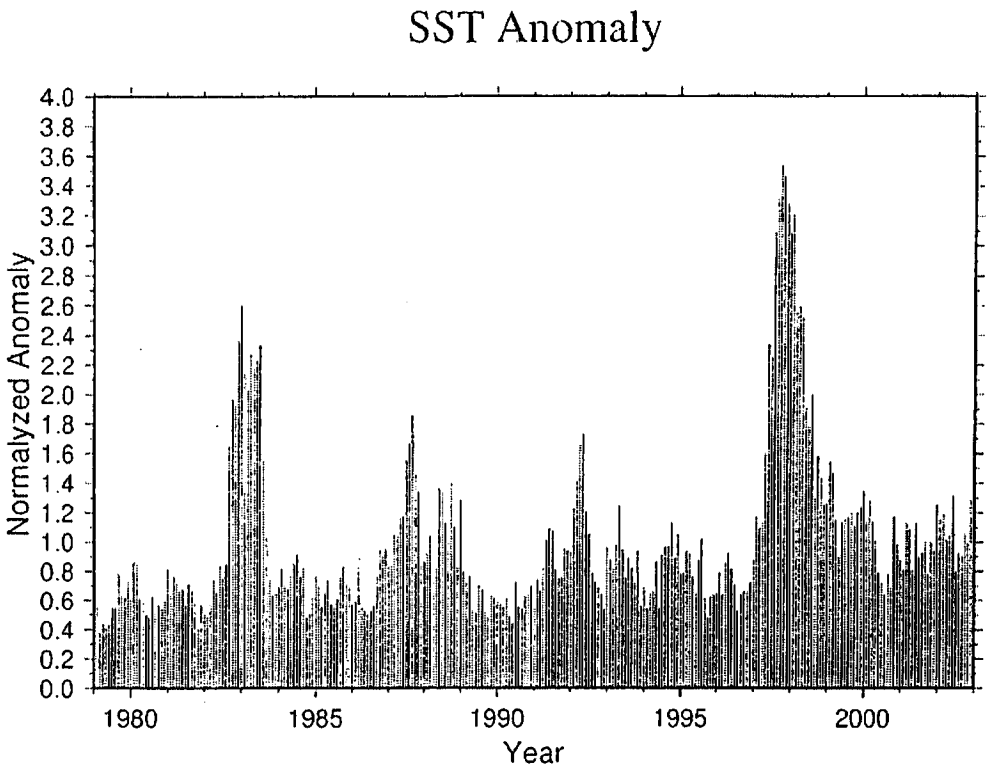

Fig. 3. The time series of the normalized SST abnormality index for 1979 to 2002.

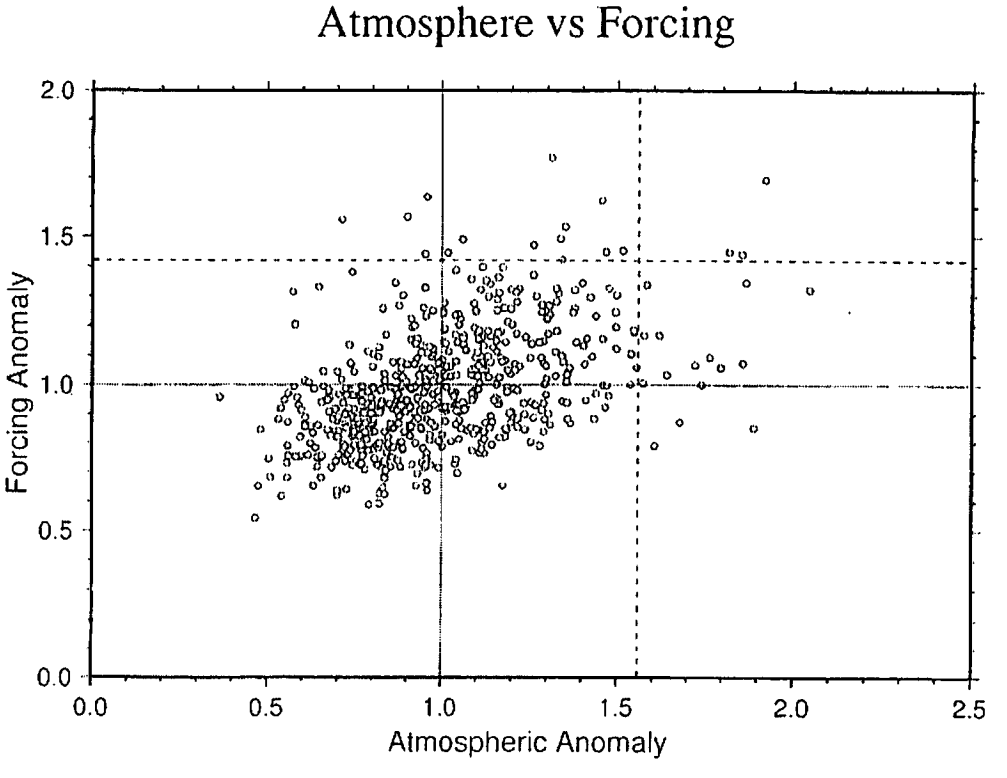

Fig. 4. The scatter diagram of the abnormality indices for the atmosphere (absissa) versus that for the forcing (ordinate) for 50 years from 1953 to 2002.